The Production of Butyl Acetate and Methanol via Reactive and Extractive Distillation. II. Process Modeling, Dynamic Simulation, and Control Strategy

ARTICLE *in* INDUSTRIAL & ENGINEERING CHEMISTRY RESEARCH · NOVEMBER 2002

Impact Factor: 2.59 · DOI: 10.1021/ie010765v

2 AUTHORS, INCLUDING:

Laureano Jiménez
Universitat Rovira i Virgili
180 PUBLICATIONS **1,198** CITATIONS

The Production of Butyl Acetate and Methanol via Reactive and Extractive Distillation. II. Process Modeling, Dynamic Simulation, and Control Strategy

Laureano Jiménez*,† and José Costa-López

Department of Chemical Engineering and Metallurgy, University of Barcelona, c/Martí i Franqués 1, 08028 Barcelona, Spain

A new process to exploit a methanol + methyl acetate mixture by reactive and extractive distillation with *n*-butanol using *o*-xylene as the entrainer has been developed. The aim of this work is to synthesize, design, and study the dynamic behavior for the azeotropic separation, the reactive and extractive distillation unit, and the solvent recovery system. The process was modeled using rate-based and equilibrium-stage approaches with the kinetic expression developed for the transesterification reaction and reported in part I of this paper (*Ind. Eng. Chem. Res.* **2002**, *41*, 6663). High-purity methanol and butyl acetate were obtained as products, and yields approaching 100% of *n*-butanol were achieved. A parametric study elucidated the effects of the key operating variables. As expected, the process bottleneck is the reactive and extractive distillation unit and, in particular, the control strategy for achieving the coupled targets. A preliminary economic study reveals that the process has no profitability.

Introduction

The combination of reaction and separation in one process unit (e.g., reactive distillation, sorption-enhanced reaction, reactive absorption, reactive crystallization), the use of technologies based on process intensification (e.g., short-path distillation, divided-wall distillation column), and process integration (e.g., recycle streams, energy/water recovery networks, utility networks) offer new potential for improving process design and have had a significant impact on revenue. The implementation of these technologies can give rise to difficulties in running and controlling the plant, but modern control techniques guarantee stable operation in most cases.

This work focuses on reactive distillation, an alternative that has received much attention in recent years. One of the major practical problems in designing reactive distillation equipment is the choice of column internals, because it is necessary to reconcile separation efficiency and catalytic activity without limiting possible column loads by pressure drop.[1] In this aspect, the work by Subawalla and Fair[2] gives detailed design guidelines for catalyzed reactive distillation systems. In addition, a complete list of references can be found in the work by Hauan.[3]

Problem Statement

Poly(vinyl alcohol) (PVA) is a water-soluble resin with adhesive, film-forming, and emulsifying properties that is resistant to oil and solvents. PVA consumption increased at a rate of almost 2% annually between 1992 and 1998. Overall PVA expenditures are forecast to remain relatively flat in the near future, indicating that most of the applications are mature.[4] PVA is manufactured using state-of-the-art control systems involving the polymerization of vinyl acetate and the partial or complete hydrolysis of the intermediate poly(vinyl acetate) to PVA and methyl acetate (MeAc) at a ratio of 1.68 tons of MeAc per ton of PVA. The main constituents of the saponification mother liquor (MM20) are methanol (MeOH) and MeAc (∼30 wt % MeAc), as well as traces of sodium acetate and acetic acid (HAc). In the past, this mixture was sold as solvent, but volatile organic compound legislation has drastically decreased this market. In the current process,[5] MM20 is fed into an extractive distillation column with water or ethylene glycol (an alternative is extraction plus distillation); MeAc and water are the top products, while MeOH and water are retrieved from the bottom. MeAc is hydrolyzed through a cation-exchange resin column or in the presence of a strong acid into HAc and MeOH. Dilute HAc is concentrated by extractive or azeotropic distillation. Sodium acetate is converted into sodium sulfate and HAc by the addition of sulfuric acid.

The unfavorable chemical equilibrium (up to 36 wt % conversion) and the azeotrope constraints (two binary azeotropes that give rise to two distillation boundaries and asymptotic VLE behavior, called a pseudoazeotrope, that implies a tangent pinch in the ternary diagram) indicate, a priori, that reactive and extractive distillation (RED) is a promising alternative. Within the process intensification philosophy, MM20 is fed to a process based on RED technology, thus integrating the whole process. MeOH is reused in the PVA process, the MM20 byproduct is revalued, and high-purity BuAc is produced. The recovered MeOH contains a small amount of acetaldehyde (from traces of acetic acid and the sulfuric acid added as homogeneous catalyst) that is converted into acetal (1,1-diethoxyethane), a component that does not affect the polymerization process, by

* To whom correspondence should be addressed. Tel.: +34-977-559617. Fax: +34-977-559667/21. E-mail: ljimenez@etseq.urv.es.

† Present address: Department of Chemical Engineering, ETSEQ, University Rovira i Virgili, Av. dels Països Catalans 26, 43007 Tarragona, Spain.

10.1021/ie010765v CCC: $22.00
Published on Web 11/16/2002

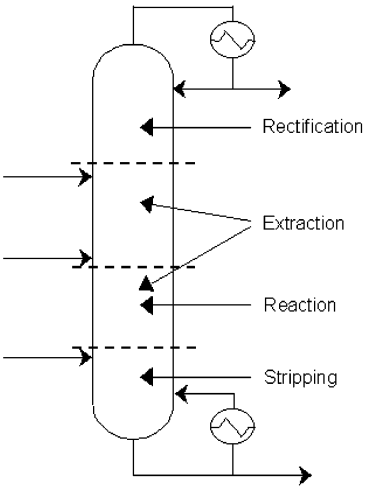

Figure 1. Typical column setup in a reactive and extractive distillation unit.

cation-exchange resins. Moreover, BuAc, an aliphatic oxygenated solvent, has not been affected by the restrictions imposed by volatile organic compounds legislation.

The reaction

$$\text{MeAc} + \text{BuOH} \leftrightarrow \text{BuAc} + \text{MeOH}$$

was studied in a batch reactor and reported in part I of this paper,[6] where a kinetic expression was obtained. In a general setup for RED, the column is usually split into four regions (Figure 1). In the reactive region, reactants are converted into products that are flushed out continuously. If the reaction is heterogeneously catalyzed, catalytic packing is used in this section. The tasks of the rectifying and stripping sections depend on the component boiling points: one is used for product purification and the other for inert and/or byproduct removal. In this case, the extractive section is located above the reactive section and also influences their behavior. Recycles can be done between any of these sections.

Simulations were performed using the commercial software tools Aspen PLUS, Dyna PLUS, Aspen SPLIT, and SPEEDUP (Aspen Technology Inc., Cambridge, MA) and its striking synergic capabilities.

A number of different issues were studied and are presented in the subsequent sections: process synthesis, process modeling, the reactive and extractive distillation unit, the solvent recovery system, dynamic modeling, and cost estimations.

Process Synthesis

This section focuses on the simultaneous analysis of the RED unit and the solvent recovery system. The physical properties of this initial phase were estimated by UNIFAC[7] with Aspen PLUS.[8]

(a) Batch/Continuous Comparison. The BuAc feasible composition for a standard distillation column is less than that obtained by the inverted procedure, where the feed is charged to the top and the heavy products are drawn from the bottom, for the same time of operation. For the standard case, a high BuAc composition cannot be achieved, even after long production periods. Thus, the standard column presents a poor performance compared to the inverted operation. Mujtaba and Macchieto[9] also recommend a complex or inverted configuration to produce BuAc by esterification.

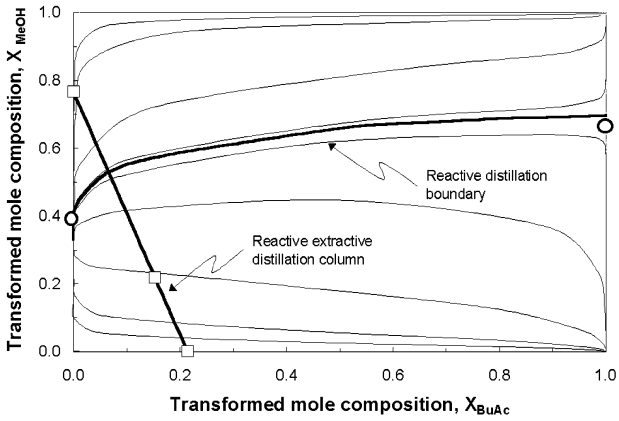

Figure 2. Reactive RCM in transformed mole composition for the transesterification of MeAc with BuOH using *o*-xylene as the entrainer at 101.3 kPa.

(b) Reactive Residue Curve Map. Several authors have transferred the reactive residue curve map (RCM) concept to reactive distillation by overlaying chemical equilibrium,[10] rate equations,[11] or homogeneously catalyzed kinetics expressions.[12] Reactive residue curve mapping shows that we can either create or eliminate distillation boundaries by modifying the RCM topology.

The calculations were performed using the reaction invariants described by Ung and Doherty[13] as stated in eq 1

$$X_i = \frac{x_i - v_i^{\mathrm{T}}(v_{\mathrm{ref}})^{-1}x_{\mathrm{ref}}}{1 - v_{\mathrm{tot}}^{\mathrm{T}}(v_{\mathrm{ref}})^{-1}x_{\mathrm{ref}}} \qquad (i = 1, ..., C - R) \quad (1)$$

where v_i^{T} is the row vector of the stoichiometric coefficients for component i in each of the R reactions, x_{ref} is the vector of mole fractions of the R reference components in the liquid phase, and C is the number of components. These new variables behave similarly to mole fractions in nonreactive mixtures (they add to unity), but they do not have to be positive. Hence, we can represent multicomponent systems in a lower-dimensional composition space ($C - R - 1$ degrees of freedom).

The nonreactive RCM calculations were performed with Aspen SPLIT.[14] BuOH was the reference component for computing the transformed molar composition shown in the reactive RCM (Figure 2). The reactive boundary generates two regions where the stable nodes are *o*-xylene and BuAc and the MeOH + MeAc azeotrope is the unstable node. In this way, the components to be separated (MeOH and BuAc) are located in different distillation regions. Fortunately, the working conditions for the reactive section, even during start-up and shutdown, lie far from this boundary. If the whole RED unit is considered (that is, in conjunction with the extractive, stripping, and rectification sections), its projection crosses the reactive boundary.[15]

(c) Process Flow Diagram. The rules from Bessling[16] are used to determine, without intensive computing, whether it is economical to separate the desired top and bottom products in just one reactive distillation column. For our system, although there is a sufficiently large difference in the pure-component boiling points ($\Delta T =$ 50 K), the equilibrium is mainly on the side of the reactants (up to 36 wt % conversion), and therefore, we conclude that more than one column is required. This result reinforces the need for an entrainer to achieve

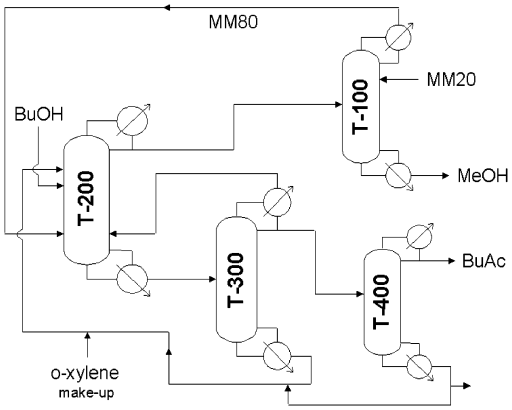

Figure 3. Schematic representation of the process. T100, azeotropic distillation column; T200, reactive and extractive distillation unit; T300, solvent recovery column; T400, BuAc purification unit.

the product specifications. Another important issue is whether it is necessary to divide the RED into reactive and nonreactive sections. In this case, it is necessary to recycle a component that is not in the reaction space (*o*-xylene) and separate the two products (MeOH and BuAc), and thus, a rectifying section and a stripping section are required. These two sections help to minimize impurities and increase the conversion. In this case, according to the literature,[2,17] a prereactor would not reduce the cost. The flowsheet can be simplified into four major unit operations (Figure 3). Crude MM20 is fed into the azeotropic distillation unit (T100) to recover the excess of MeOH (helping the chemical equilibrium forward). The top product, MM80, is the binary azeotrope MeOH + MeAc and is fed to the RED unit (T200), where *o*-xylene and BuOH are also supplied. Any heavy impurity that is recovered from the top of T200 contaminates the MeOH, whereas any light impurity in the bottom affects the performance of the solvent recovery system. The solvent recovery system has two distillation columns: T300 and T400. The *o*-xylene is recycled to T-200.

Process Modeling

The following factors that determine the overall system behavior were thoroughly studied: (a) vapor−liquid equilibrium, (b) reaction kinetics, (c) mass-transfer issues, (d) separation efficiency, (e) convergence, (f) trace impurities, and (g) equilibrium-stage versus rate-based approach.

(a) Vapor−Liquid Equilibrium. The models and parameters used to estimate the physical properties can be found in part I of this paper.[6] The vapor pressures were derived from an expanded Antoine equation. All other values used were retrieved from the Aspen PLUS database.[8]

Process simulation does not alleviate the need for accurate physical property data and models.[18,19] This issue becomes particularly important when the product specifications are based on the maximum impurities at trace levels. In particular, pseudoazeotrope behavior for methanol + *o*-xylene was detected at high concentrations. VLE prediction capabilities were tested for the five-component system ($\overline{\Delta T}$ = 1.4 K, ΔT_{max} = 3.4 K, Δy_{max} = 0.0184, and the root-mean-square deviation of the vapor mole fraction was 0.058%).

(b) Reaction Kinetics. Chemical equilibrium and kinetics were studied extensively in part I of this paper.[6] A recent work by Pöpken et al.[20] shows that it is not clear whether homogeneous or adsorption-based kinetics better describes the column performance. A pseudohomogeneous model (eq 2) was found to be adequate for predicting the reaction rates within 1−2% estimation error

$$r = 2.018 \times 10^8 \exp(71\,960/RT) c_{\mathrm{MeAc}} c_{\mathrm{BuOH}} - 2.839 \times 10^8 \exp(72\,670/RT) c_{\mathrm{BuAc}} c_{\mathrm{MeOH}} \quad (2)$$

where r is the reaction rate (mol·L^{-1}·min^{-1}·g$_{cat}^{-1}$) and c_i is the concentration (mol·L^{-1}).

The reaction rate was calculated on the basis of the amount of catalyst on each stage, thus avoiding the complex computation of the liquid hold-up, which is strongly dependent on the components, the system hydrodynamics, and the operating conditions.

Because of the negligible thermal effects associated with the reaction, the catalyst particles were essentially isothermal. Because the product specifications for the MM20 produced were a maximum water content of 0.05 wt % and a maximum acidity of 0.05 wt %,[5] the presence of any byproduct was experimentally determined (e.g., acetic acid).

(c) Mass-Transfer Issues. In part I of this paper,[6] experimental work was completed to ensure that the kinetic expression was free of mass-transfer effects. DeGarmo[21] reported that the mass-transfer efficiency of catalytic structured packing is almost equivalent to that of a conventional structured packing. This work also stated that the catalyst efficiency, expressed as a percentage of the rate in a stirred reactor, is greater than 75% throughout the typical operating range. This effect was considered in the rate-based models, but as shown in the process modeling section, no influence was detected.

Amberlyst 15, a sulfonic ion-exchange resin manufactured by Rohm & Haas (Philadelphia, PA), was used as the catalyst. The heterogeneous catalyst was immobilized between two packing sheets (BX metal gauze, Sulzer, Winterthur, Switzerland), forming a sandwich-like structure. All catalyst slices were assumed to be fully wetted. Because the catalyst pellets are very small (less than 1 mm in diameter), capillary action tended to hold liquid in the interstitial spaces within the catalyst bed. Any other packing used was stainless steel Fleximax (Koch-Glitsch, Wichita, KS), except for T100, where sieve trays were used (single-pass).

(d) Separation Efficiency. It is well-known that the separation efficiency of structured packing diminishes with increasing surface tension of the liquid because of poor wetting.[22] In this case, the surface tension in the reactive section remained relatively constant, with a maximum deviation of 3.5%.

Vendor data[23] and data retrieved from the literature[24] were used to set the characteristics of the packing. According to this information, no significant dependence on the separation efficiency for the pressure and internal liquid/vapor flows in the reactive zone should be detected for the foreseen operating conditions. This information was used in the subsequent design. Results from rate-based models confirmed this assumption.

(e) Convergence. To improve the convergence, the tear streams were selected according to partition and decomposition algorithms.[8] The recycle loops were highly interrelated, and the Broyden method was chosen to

accelerate convergence. For nested loops (e.g., T200−T300 and T200−T400), the inner-loop tolerance was fixed to be tighter than the outer-loop tolerance. The streams selected were the top product from T200, the total *o*-xylene recycled, and the light impurities retrieved from the top of T300. A gradually relaxed convergence test was selected to avoid the unstable behavior of the trace components that affects the stability of the loops. Details about the algorithm used to solve the column equations can be found in the work by Venkatamaran et al.[25] Also, a Fortran block was introduced to fix the exact solvent makeup dynamically.

(f) Trace Impurities. Purge streams were introduced to remove the heavy impurities in the entrainer recycle stream. Any light impurity leaving T200 at the bottom was recycled back from the T300 top product; in particular, during start-up, a significant amount of this stream was sent back to T200 until normal operating conditions were achieved.

(g) Equilibrium-Stage versus Rate-Based Approach. Equilibrium-stage (RADFRAC) and rate-based (RATEFRAC) model predictions were compared in the RED. The major advantage of the second option is that empirical factors, such as efficiency or height equivalent to a theoretical plate (HETP), are completely avoided. For reactive distillation, the estimation of HETP is very difficult, and there is experimental evidence[26] that the efficiency can have any positive, zero, or negative value with almost no change in the hydrodynamic conditions. As a consequence, only the main components (e.g., MeOH and MeAc in T100, BuAc and *o*-xylene in T300) were considered to compute the stage efficiencies. The correlations used for mass-transfer coefficients, interfacial areas, and heat-transfer coefficients can be found in ref 7. Heat losses were computed according to a linear model, as was found experimentally by Pöpken et al.[20]

Recently, Ellenberg[22] measured residence time distribution for structured packings similar to those selected in this case (Sulzer BX and Koch Fleximax), and conditions close to plug flow for the liquid phase were found. The reactive section of the column was treated as a plug-flow reactor in series by dividing each column segment into a number of slices (in this case 15). For a second-order reaction, the reaction extent should depend on the residence time distribution. This issue was investigated with the rate-based model (variations up to ±10%), but no significant effect was detected; that is, although the reaction rate was modified in all stages, the total reaction rate remained almost constant. Ellenberg et al.[22] also disregarded this effect.

Predictions for the bulk-phase temperature using a rate-based model are virtually the same as those from the equilibrium-based model ($\overline{\Delta T}$ = 1%, $\overline{\Delta x}$ =1%, and Δy_{max}=3.5%). We conclude that, for the column diameters involved, the small differences detected do not justify the use of such a complex model. For larger diameters, this effect must be reconsidered.

Reactive and Extractive Distillation Unit

For the simulation, the reboiler duty, feed flow rates, and reflux ratio were specified in the same way as they are usually fixed as operating conditions. Stages were numbered top-down, with stage 1 being the condenser and stage *N* the reboiler. The simulation contained no adjustable parameters.

Because of the complex interactions between the chemical reaction and the separation, the performance of RED columns is influenced by several parameters, e.g., reflux ratio, column diameter, pressure, sizes of reactive and nonreactive sections, feed stage location, and entrainer ratio.[27,28]

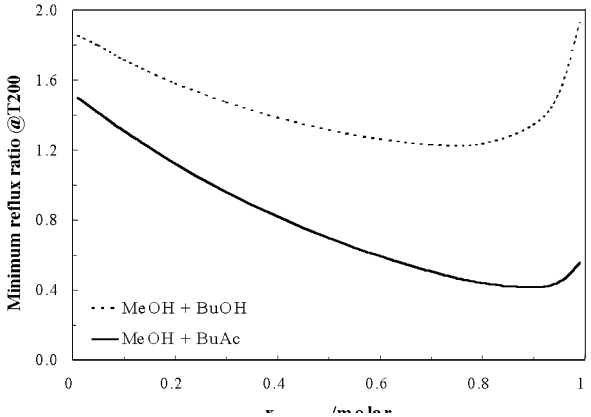

Figure 4. Influence of the entrainer feed flow rate on the reflux ratio for the key separations.

(a) Reflux Ratio. At low reflux ratios, insufficient product separation limits the conversion, and traces of heavy component contaminate the T200 top product. At high reflux ratios, the reactants are separated too effectively (i.e., the profiles do not match), thus limiting conversion. Moreover, as stated in the Reactive Residue Curve Map section, if a low conversion is achieved, the top product is the MeOH + MeAc minimum-boiling azeotrope. The optimal reflux ratio is a compromise solution between these situations, although it has been shown that reacting reflux ratios are higher than nonreacting.[2,17] When the reflux ratio was varied, a parabolic profile with more than 90% conversion at reflux ratio between 2.2 and 3.4 was found. The maximum was located around 3. Fortunately, a flat minimum was obtained (Figure 4).

(b) Column Diameter. The column diameter was rated using both the maximum capacity factor[8,24] and the flooding percentage,[24,29] to check predictions and/or correlation inaccuracies. Typically, each vendor[4] uses an in-house method to define the maximum capacity; in this case, a maximum flooding of 75% and vendor-recommended[23] pressure drop of ∼12 mbar·m^{-1} were used as design criteria. The most conservative value of both methods was selected, and the RED column diameter was set to 0.55 m. Columns with variable diameters were rejected because the maximum divergences considering all column sections were about 8%.[24] Calculations were performed with rate-based models, and the efficiencies were back-calculated from a rigorous analysis of the hydrodynamic conditions.[8,25]

The internal vapor flow was reduced below the reactive section because low-boiling MM80 enters the column in this section, and some vapor was condensed to supply the heat of vaporization (slightly higher than the amount corresponding to the internal vapor flowing up the column). Also, the slightly endothermic heat of reaction (∼10 kJ·mol^{-1}) favored this issue.

(c) Operating Pressure. If the pressure was increased, a lower separation at the stripping and rectifying sections could be achieved, whereas the catalyst constrained the maximum operating temperature. Thus, atmospheric pressure was fixed in the condenser. The pressure drop was computed from generalized correlations[23,24] that were introduced in the model.

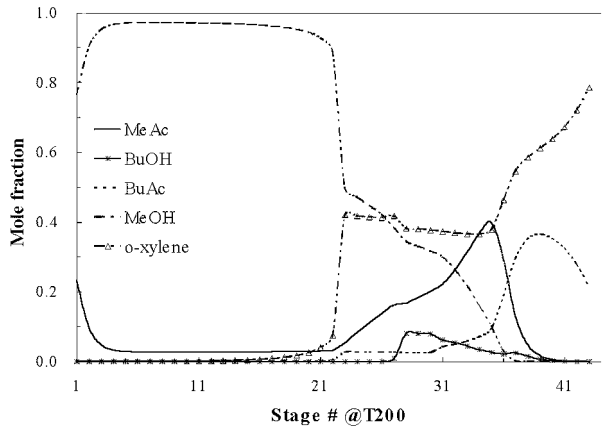

Figure 5. Composition profile in the T200 reactive and extractive distillation column.

(d) Sizes of Reactive Stages and Nonreactive Sections. As expected, the reaction had an important effect on the volatilities in the reactive section (if no reaction occurred, volatilities exhibit a smooth and predictable profile). In particular, the volatility of MeOH increased dramatically, whereas the volatility of MeAc exhibited a maximum. Moreover, the entrainer influence increased both the MeAc and MeOH relative volatilities, although the change was more important for the latter, thus improving the separation. The BuOH volatility remained relatively flat in the extractive section but increased in the reactive section. This led to a situation in which the reactant composition profiles did not exactly match: MeAc exhibited a maximum in the reactive section, whereas unreacted BuOH was internally recycled from the stripping section of the column (Figure 5).

The effect of the weight hour space velocity (WHSV), which is calculated by dividing the total mass flow rate to the column by the mass of the catalyst, was investigated.[30] The BuOH yield was practically constant for normal operating values, where WHSV is between 22 and 30 $g_{BuAc}\cdot h^{-1}\cdot g_{cat}^{-1}$. Within this range, the amount of catalyst was large enough to hydrate most of the reactants fed to the column. For values higher than 35−38 $g_{BuAc}\cdot h^{-1}\cdot g_{cat}^{-1}$ some unreacted BuOH appeared in the bottom stream; hence, any additional increment is counterproductive. As essentially no influence from the reverse reaction was detected (Figure 5), near-total conversion did not require a considerable increase in the number of reactive stages. For the rest of this paper, six reactive stages were used. Each stage contained 3.72 kg of catalyst (∼20% of the void volume).

Additional simulation runs were performed to check the effect of nonreactive stages.[31] It was found that five nonreactive stages were needed below the catalytic packing (stripping section) to recycle the unreacted BuOH back to the reactive section. The extractive section had 5 stages, and 23 additional stages were necessary for the rectifying section to minimize the top impurities.

(e) Feed Stages. Simulation results show that the conversion depends less on the number of reactive stages than on the use of three different feed stages (MM80, BuOH, and *o*-xylene). The influence of the feed stage was check by sensitivity analysis, and key results were computed (conversion, energy needs, top and bottom impurities). When reactant feeds were located inside the reactive region, a relatively low conversion was achieved. The conversion increased and reached a maximum when the feed flows were located directly below and above the reactive section of the column (stage 28 for BuOH and stage 36 for MM80). The entrainer was fed to stage 23 to ensure their flow through the reactive section. As conversion was virtually complete, no pump-around was considered.

The column exhibited a remarkable increase in the stage temperature below the reactive section. This circumstance will have a major impact in the control strategy section. To minimize this effect , MM80 was fed partially vaporized, improving the temperature stability of the reactive section.

(f) Feed Ratio. As expected, the global BuOH/MeAc molar ratio was approximately stoichiometric (0.99 mol). A high conversion was achieved because MeAc losses from the top were recycled after being reprocessed by T100, leading to a 45% MeAc excess in T200. Concerning the entrainer, the molar ratio with MM80 was fixed at approximately 2 in the first part of this paper.[6] Table 1 shows the operating conditions, as well as the range of values at which each parameter was evaluated. A large number of sensitivity analyses with cross-linked variables were carried out.

Table 1. Operating Conditions Used for the Simulation of the Reactive and Extractive Distillation Column (T200)

parameter	base case	range evaluated
reflux ratio	3.0	1.5−3.5
diameter (m)	0.55	unchanged
F factor (%)	50	80
pressure (kPa)	101	101−250
no of reactive stages	6	4−11
no of stripping stages	5	4−10
rectifying stages	30	20−33
entrainer feed stage	23	20−26
MM80 feed stage	36	33−39
BuOH feed stage	28	25−31
entrainer/MeAc ratio (mol %)	1.98	1.8−2.2
BuOH/MeAc ratio (mol %)	0.988	0.98−1.02
WHSV ($g_{feed}\cdot h^{-1}\cdot g_{cat}^{-1}$)	26	20−40
reboiler load ($kJ\cdot s^{-1}$)	149.6	unchanged
condenser load ($kJ\cdot s^{-1}$)	137.5	unchanged

Solvent Recovery System

All minimums detected (Figures 4 and 6−8) were relatively flat, thus acting as ranges for optimization and not as hard specifications. For a base case, sensitivity analyses were carried out, with each parameter being changed over a wide range. For instance, the feed stages in columns T300 and T400 were optimized according to the energy cost. The optimum feed for column T300 was stage 20, whereas for T400 (Figure 6), the liquid and vapor feeds were set to stages 30 and 28, respectively.

T300 and T400 were investigated to fix the optimum recycle flow rate and composition. With respect to the BuAc recovery at T300 (Figure 7), the mathematical optimum was around 78.5%. In this case, a compromise solution between product recovery and energy load was taken into account, because the solvent recovery system consumes 46% of the total energy load, and it is unnecessary to purify any recycle stream.[2] On the other hand, high reflux flow rates were involved in the T200−T300 system. The recycle flow rate from T400 (Figure 8) was fixed at 0.445 $kmol\cdot h^{-1}$, a value lower than the mathematical optimum.

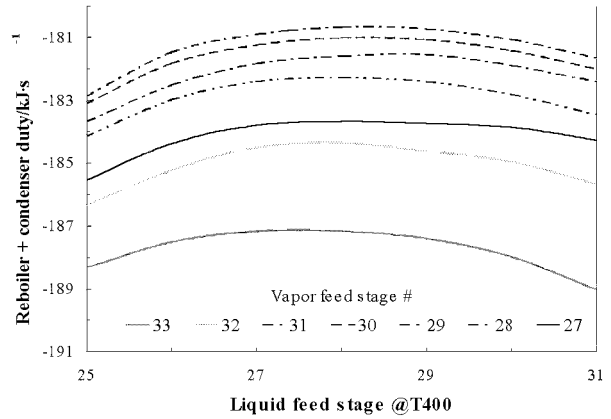

Figure 6. Sensitivity analysis to detect the optimum feed stages for T400.

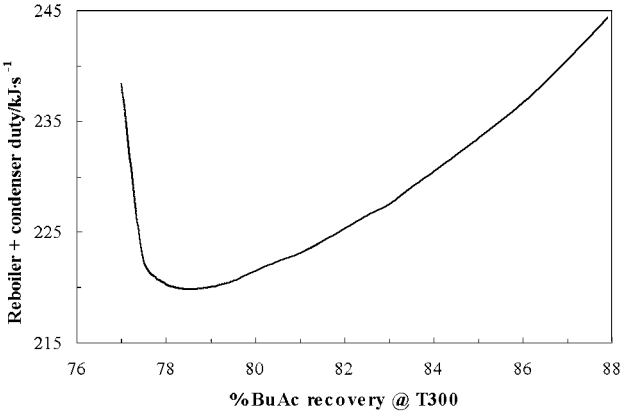

Figure 7. Sensitivity analysis to detect the optimum BuAc recovery for the T300 distillation column.

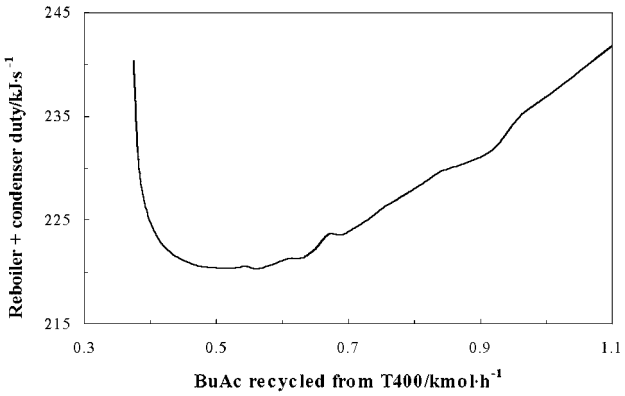

Figure 8. Sensitivity analysis to detect the optimum BuAc recycled from the T400 distillation column.

Sensitivity analyses were performed for different subsystems (e.g., T100 + T200; T200 + T300) as a partial optimization tool. Four parameters were allowed to vary per case, each one in a three-level experimental design (i.e., high, medium, and low), thus leading to 256 runs. Also, different combinations of variables were used for the same system (e.g., feed stages and number of stages or reflux ratio and recoveries). The criteria were the equipment cost and the total energy load, thus aiming at a compromise with capital and operation costs. For example, the MeOH impurities in T100 and the BuOH conversion are very sensitive to the BuOH and *o*-xylene feed temperatures in T200. As both influences have a reverse effect, the best solution was to set the entrainer feed temperature to 65 °C and the BuOH temperature to 66 °C. The optimal configurations for T100 feed stages are 9 and 11 for MM20 and the top product from T200, respectively. Nevertheless, the energy savings (1045 $J \cdot s^{-1}$) were not enough to compensate for the additional feed stage required, and both feeds were located on stage number 10. The global results for T100, T300, and T400 are shown in Table 2.

Table 2. Operating Conditions for the Distillation Columns in the MeOH Purification (T100) and the Solvent Recovery System (T300 and T400)

parameter	T100	T300	T400
reflux ratio	2.0	7.0	5.2
diameter (m)	0.40	0.40	0.40
pressure (kPa)	101	101	101
no. of stages	30	30	40
feed stage	10, 10	20	28, 30
reboiler load ($kJ \cdot s^{-1}$)	97.4	126	88.6
condenser load ($kJ \cdot s^{-1}$)	66.0[a]	122[a]	92.4

[a] Partial condenser.

Dynamic Modeling

The presence of multiple steady states, as is well-known in MTBE production,[32] can greatly complicate the operation of a distillation column. In this study, no multiplicity was detected.

Because no differences between the rate-based and equilibrium-stage models were observed for the steady state, the latter model was used for dynamic modeling. Dyna PLUS[33] and SPEEDUP[34] were used to perform the task automation and manage the dynamic events. The initial conditions were fixed as the steady-state stationary values. The theoretical VLE compositions were corrected by introducing the average efficiency from the rate-based model. The dynamic degrees of freedom (e.g., level and hold-up) were fixed at 50%. Reflux drums and intermediate reservoirs were modeled as continuous stirred tanks, thus minimizing error propagation and helping to achieve smooth operation. No time considerations were implemented for the start-up period, and therefore, the steady state was reached instantaneously. Balances in the reboiler and condenser were also instantaneous. Logarithms of the mean temperature differences for steam (2 or 11 atm) and cooling water (20 °C) were used to perform the calculations. During simulations, the pressure drop was automatically updated according to the vendor procedure.[8,23]

Very strong influence of various parameters were detected.[35] This highly coupled system performance is due to the complex interactions between VLE, reaction kinetics, and column hydraulics, leading to the complex dynamic operation of the RED unit.[36] To minimize the coupling (e.g., T100−T200), multivariate control techniques are needed, which is far beyond the scope of this work.

To develop the control structure and tune the control parameters, the recycle streams were fixed as inlet streams. Fine-tuning and robustness analyses were conducted in the closed-loop system. The dynamic behavior with regard to common process upsets was studied to detect phenomena that can lead to severe control problems (e.g., transient behavior or inverse responses).

(a) Control Structure. Decentralized control systems have fewer adjustable parameters and are easier to understand and tune than general multivariable controllers. The inadequacies of conventional procedures

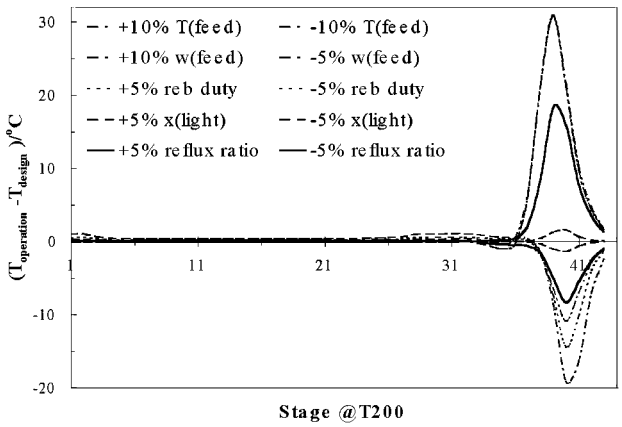

Figure 9. ΔT profiles for typical process upsets in the T200 distillation column.

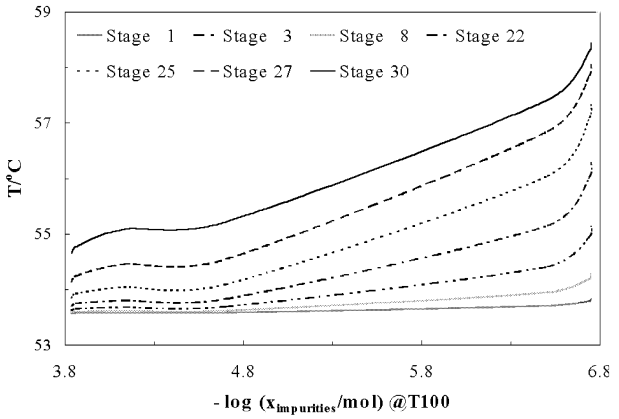

Figure 10. Impurity analysis results for typical process upsets in the T100 distillation column.

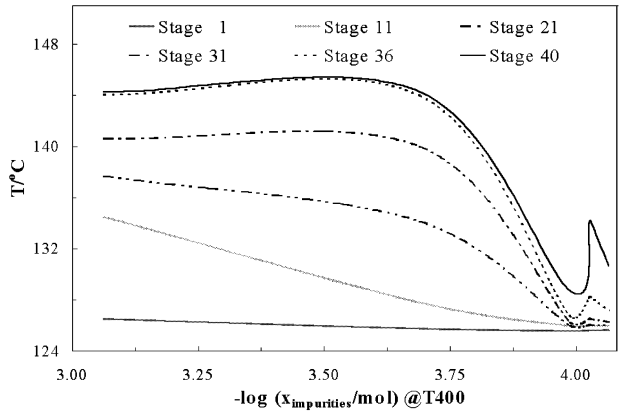

Figure 11. Impurity analysis results for typical process upsets in the T400 distillation column.

with single-input single-output pairing based on steady-state results highlight the need for controllers designed on the basis of dynamic models.[37]

As pointed out before, the main process constraints are the operating conditions for the RED unit (T200): heavy impurities recovered overhead and light impurities leaving by the bottom stream will contaminate the MeOH and BuAc, respectively. Additionally, the controller structure was constrained for the catalyst temperature in the reactive section.

Ratio controllers minimize equipment coupling, upset propagation, and compensate disturbances because input variables change proportionally in a feed-forward control strategy. The MM20 variation in composition was very small, and stoichiometric ratio controls for reactants (0.30 BuOH/MM20 by weight) and for the entrainer/MM20 ratio were set (2.23:1 by weight). The entrainer recycle stream was also adjusted with the T300 feed flow rate.

To establish the control structure, common strategies for reactive, extractive, and azeotropic distillation had to be combined.[38,39] Differences in temperature profiles (ΔT versus stage) were examined to determine the control performance for temperature (best sensor location, sensitivity). As expected, the T200 top temperature (Figure 9) was not sensitive. Figure 9 also shows that, no matter which disturbance (up to ±10%) is introduced into the system, the temperature in the reaction section remains constant. Below this section, important temperature variations were detected. This analysis corroborates that a small vapor fraction in MM80 minimizes the temperature variability in the reactive section. Because of catalyst deactivation, the reboiler duty was controlled with the reactive section average temperature (stages 38−40). To avoid coupling with the feed inlet located between them, the reboiler duty was cascaded with the temperature in stage 36 as a secondary variable. Within this control scheme, the controller was not saturated by the temperature variability. Because of the closeness of the manipulated and the controlled variable, this control loop was relatively fast.

For distillation columns where high-purity components were obtained (T100 and T400), total impurities analyses[38] were investigated because the product stream temperatures were not sensitive. In these diagrams, the logarithms of the mole fractions of the impurities versus the temperatures are plotted for typical upsets. These diagrams show whether direct or indirect action can be fixed (Figure 10). Figure 11 shows that T400 exhibits a reverse behavior: some upsets increase the temperature, whereas others reduce it. No inferential strategy was found, so to overcome these situations, an on-line analyzer was used. Using the aforementioned insights into the dynamics, an efficient control structure was presented for the strongly nonlinear coupled system of the RED unit (Table 3).

Table 3. Control Configuration for the Reactive and Extractive Distillation Unit (T200)

manipulated variable	controlled variable	K_c	τ_I (min)	τ_D (min)
bottom flow rate	reboiler level	1.2	5.4	
top flow rate	reflux drum level	5.1	7.8	
cooling water flow rate	top pressure	9.2	8.2	1.1
vapor flow rate (cascaded)	average temperature (stages 38−40)	12	26	0.64
cascaded	temperature at stage 36	1.1	5.2	

(b) PID Algorithms. Standard PID controllers with derivative filters were used to minimize the effect of the signal noise. The on-line analyzers were modeled as first-order systems with time lags of 5 min. Temperature and pressure sensors were assumed to be instantaneous, although typical time constants are around 30 s. Dyna PLUS assumed first-order behavior on the Laplace domain for the measured variable. As a general rule, we can state that the instability is favored when the gain (K_c) increases and the derivative time (τ_D) and integral time (τ_I) decrease.

(c) Parameter Tuning. The autotuning value (ATV) method was easily implemented, as no preliminary knowledge of the system dynamics was needed. To

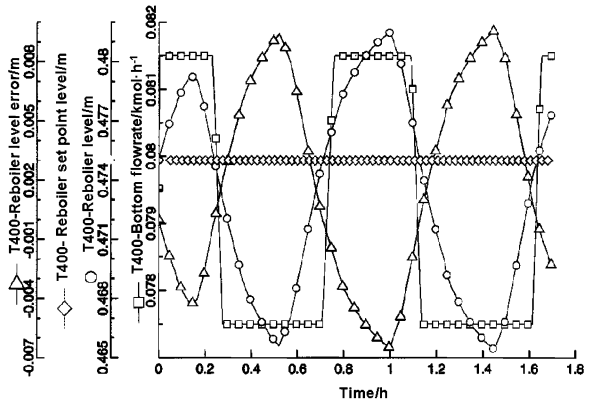

Figure 12. ATV method for the reboiler level control in the T400 distillation column.

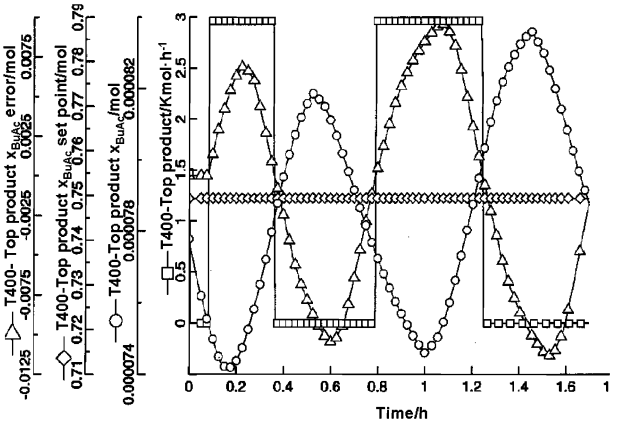

Figure 13. ATV method for the top product purity control in the T400 distillation column.

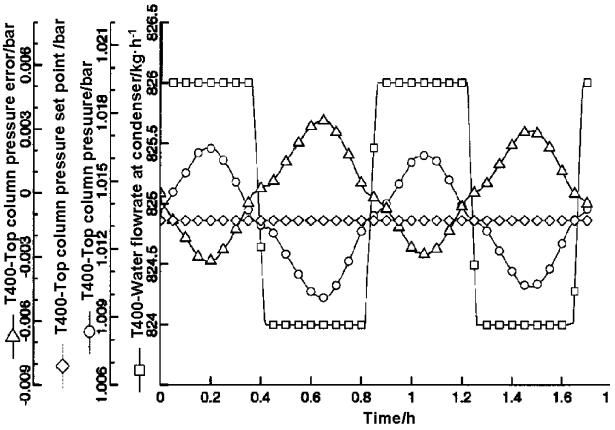

Figure 14. ATV method for the pressure in the T400 distillation column.

perform the ATV method,[38] the integral and derivative actions were deactivated, and the gain was set to infinity. Also, the maximum and minimum control actions were fixed in a narrow range around the set point. Figures 12−14 show the typical system behavior of T400 resulting from a small disturbance in the set point, in which the target variable changes using a sequence of pulses (switching instantaneously from the maximum to the minimum action), whereas the operation variable exhibits a harmonic performance. On the basis of the oscillating response and the Ziegler−Nichols method, preliminary controller parameters were calculated. Straightforward controllers were tuned according to the open or closed Ziegler−Nichols methodology.[38]

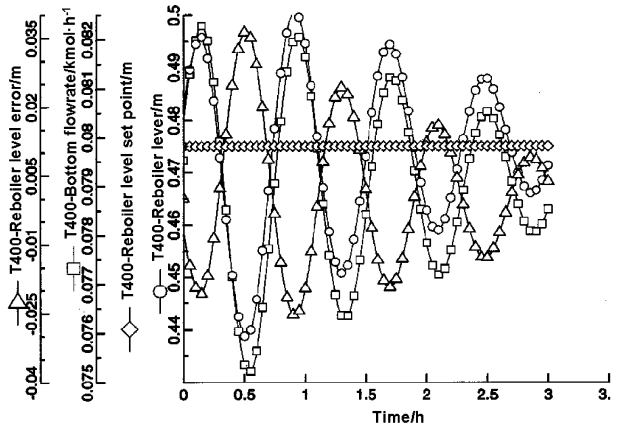

Figure 15. T400 reboiler level performance for a 5% increase in feed temperature.

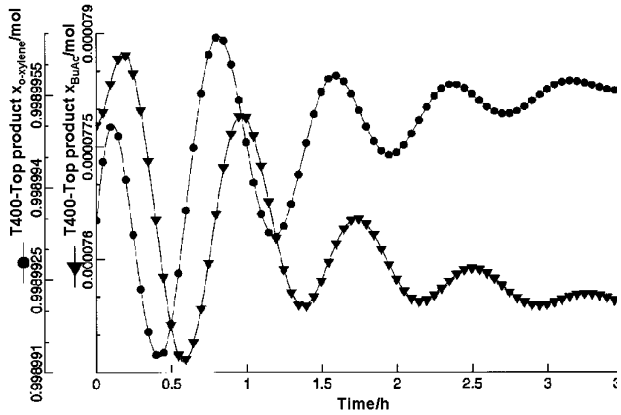

Figure 16. T400 top composition performance for a 5% increase in feed temperature.

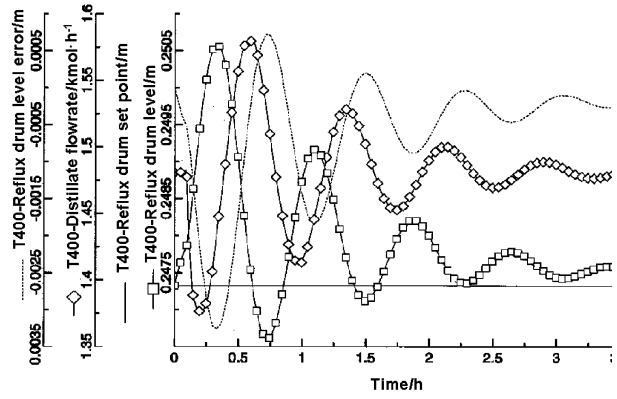

Figure 17. T400 reflux drum level performance for a 5% increase in feed temperature.

(d) Robust Control. The design of any control system involves, either explicitly or implicitly, a model that describes the real system. Analyses of the performance resulting from typical upsets in process variables (again, up to ±10%), such as feed flow rate, feed pressure, feed temperature, feed composition, reflux flow rate, reboiler duty, refrigeration water flow rate, and operating pressure, were carried out to check the model robustness. For example, the closed-loop behavior for T400 is analyzed in Figures 15−17. As shown, the top composition, the reflux level, and the bottom level behaviors are stable for a pulse upset in feed temperature (+5%). Typical upsets do not have a strong effect on the conversion achieved in T200, because reaction rates increase in some stages while decreasing in others.

As expected, column behavior was detected to be asymmetric in most cases. That is, the behaviors for disturbances of, say, +5% and −5%, in a process variable (e.g., pressure or flow rate) did not exhibit reverse and symmetric effects on the measured variable (e.g., composition or level). Some reverse transient behaviors were detected when a perturbation was introduced into the system. For instance, when the reflux ratio was decreased in T200, the temperature in the reactive section temperature reached a maximum after around 20 min. When feed temperature variations were introduced into T200, the system behavior was similar, but with a slower response. Similarly, the top composition and flow rate in T400 experienced reverse transient phenomena when the feed temperatures were increased. In those cases, great care was taken to select the input/output pairing variables.

Cost Estimation

A modular cost estimation to assess the process profitability was performed. First, the basic cost of unit operations were estimated using indexes taken from *Chemical Engineering*, *Oil and Gas Journal*, *Engineering News-Record*, and Marshall and Swift.[8] Then, a set of indexes for each type of unit operation (e.g., pumps, distillation columns) was used to weigh direct and labor costs (e.g., concrete, electrical, piping). Labor, inflation, and utilities costs from Spain were used. The costs of all chemicals were obtained from the *Chemical Market Reporter*,[40] considering the average of a 6-month period. As reactive distillation units are not common in industry, a relatively high contingency factor was arbitrarily fixed (i.e., 20%). Cost estimation was divided into four steps: unit operations costs (1.32×10^6 U.S.$), operating costs ($2.5 \times 10^5$ U.S.$/year), fixed costs (separated into direct costs, 3.79×10^5 U.S.$; indirect costs, 6.79×10^5 U.S.$; and contingency costs, 6.64×10^5 U.S.$), and project profit.

The economic analysis shows that the RED process has no profitability by itself. In particular, a more extensive and realistic analysis that compares the actual process (conversion into diluted acetic acid) with the proposed solution reveals that the RED approach has fewer losses, but the high capital penalty still favors the current alternative. It is important to point out that this work explores an alternative process for a waste stream, and in such cases, it is very difficult to find any cost-effective alternative.

Conclusions

Modeling indicates that it is possible to obtain very high-purity BuAc and MeOH from a process based on RED. Because the chemical reaction changes the topology of the RCM, new options for separation were found. Although VLE and kinetics agree with the experimental data, pilot-plant data are strongly recommended to validate simulation predictions. For the column diameters and operating conditions involved, the equilibrium-stage concept is sufficient to model the column behavior. The effects of the reflux ratio, sizes of reactive and nonreactive sections, feed stage location, and entrainer ratio were studied for the RED unit. Moreover, the performance of the solvent recovery system was optimized.

A control loop that yields good performance with stability in the high-purity region was developed. As expected, nonsymmetric behaviors were detected for most variables. The major control problems for RED were found in the multiple objectives (total conversion, maximum temperature in the reactive section, top and bottom maximum impurities, and feed ratios). The performance of the system for typical upsets was far beyond the expectations, as the system remains stable in all cases.

Some key results are a BuOH conversion of 99.91%, a MeOH purity of 99.82%, an *o*-xylene content in MeOH of 15.2 ppm, a BuAc purity of 99.81%, an *o*-xylene content in BuAc of 51.2 ppm, a heat utility of 183.9 MJ/ton MeOH, and a cold utility of 180.2 MJ/ton MeOH.

Acknowledgment

The authors thank DGICYT, CIRIT, and AspenTech HQ for providing the necessary facilities. L. Jiménez gratefully acknowledges financial support from Fundación Caja de Madrid.

Notation

ATV = autotuning value
BuAc = butyl acetate
BuOH = butanol
c_i = molar concentration, $mol \cdot L^{-1}$
C = number of components
HAc = acetic acid
HETP = height equivalent to a theoretical plate, m
K_c = gain
MeAc = methyl acetate
MeOH = methanol
MM20 = mother liquor from the PVA process
MM80 = MeOH + MeAc azeotropic mixture from the PVA process
PVA = poly(vinyl alcohol)
r = reaction rate, $mol \cdot L^{-1} \cdot min^{-1} \cdot g_{cat}^{-1}$
R = number of reactions or universal gas constant, 8.314 41 $J \cdot mol^{-1} \cdot K^{-1}$
RCM = residue curve map
RED = reactive and extractive distillation
T = temperature, °C or K
VLE = vapor−liquid equilibrium
WHSV = weight hour space velocity, $g_{feed} \cdot h^{-1} \cdot g_{cat}^{-1}$
x_{ref} = vector of mole fractions of the R reference components in the liquid phase
x_i, y_i = liquid and vapor phase mole fractions, respectively
X_i, Y_i = transformed liquid and vapor mole fractions, respectively

Greek Symbols

γ_i = liquid-phase activity coefficient
Δ = increment
τ_D = derivative time, min
τ_I = integral time, min
v_i^T = row vector of the stoichiometric coefficients for component i

Subscripts and Superscripts

i, j = ith and jth components, respectively
max = maximum
ref = reference component
s = mean value

Literature Cited

(1) Taylor, R.; Krishna, R. Modelling Reactive Distillation. *Chem. Eng. Sci.* **2000**, *55*, 5183.

(2) Subawalla, H.; Fair, J. R. Design Guidelines for Solid-Catalyzed Reactive Distillation Systems. *Ind. Eng. Chem. Res.* **1999**, *38*, 2696.

(3) Hauan, S. http://www.andrew.cmu.edu/user/steinhau/Literature/access.html (accessed July 2002).

(4) William, J.; Humphries, G.; Sakota, K. Polyvinyl Alcohol CEH Report. Available at http://ceh.sric.sri.com/Public/Reports/580.1810/ (accessed July 2002).

(5) Erkol Homepage. Available at http://www.erkol.com/ (accessed July 2002).

(6) Jiménez, L.; Garvín, A.; Costa-López, J. The Production of Butyl Acetate and Methanol via Reactive and Extractive Distillation. I. Chemical Equilibrium, Kinetics, and Mass-Transfer Issues. *Ind. Eng. Chem. Res.* **2002**, *41*, 6663.

(7) Gmehling, J.; Li, J.; Schiller, M. A Modified UNIFAC Model 2. Present Parameter Matrix and Results for Different Thermodynamic Properties. *Ind. Eng. Chem. Res.* **1993**, *32*, 178.

(8) AspenTech. *Aspen PLUS Reference Manual for Release 10*; Aspen Technology Inc.: Cambridge, MA, 1998.

(9) Mujtaba, I. M.; Macchietto, S. Design of Operation Policies for Batch Distillation. In *Batch Processing Systems Eng: Fundamentals and Applications for Chemical Engineering*; Nato ASI Series F Computer and System Sciences; Reklaitis, G. V., Ed.; Springer-Verlag: Berlin, 1996; pp 174−215.

(10) Barbosa, D.; Doherty, M. F. The Influence of Equilibrium Chemical Reactions on Vapor−Liquid Phase Diagrams. *Chem. Eng. Sci.* **1988**, *43*, 529.

(11) Solokhin, A. V.; Blagov, S. A.; Serafimov, L. A. Open Evaporation Processes Accompied by Chemical Reaction in the Liquid Phase. *Theor. Found. Chem. Eng.* **1990**, *24*, 103.

(12) Venimadhavan, G.; Buzad, G.; Doherty, M. F.; Malone, M. F. Effect of Kinetics on Residue Curve Maps for Reactive Distillation. *AIChE J.* **1994**, *40*, 1814.

(13) Ung, S.; Doherty, M. F. Synthesis of Reactive Distillation Systems with Multiple Equilibrium Chemical Reactions. *Ind. Eng. Chem. Res.* **1995**, *34*, 2555.

(14) AspenTech. *Aspen SPLIT Reference Manual for Release 1*; Aspen Technology Inc.: Cambridge, MA, 1998.

(15) Jiménez, L.; Wahnschafft, O. M.; Julka, V. Analysis of Residue Curve Maps of Reactive and Extractive Distillation Units. *Comput. Chem. Eng.* **2001**, *25*, 635.

(16) Bessling, B.; Löning, J. M.; Ohligschläger, A.; Schembecker, G.; Sundmacher, K. Investigations on the Synthesis of Methyl Acetate in a Heterogeneous Reactive Distillation Process. *Chem. Eng. Technol.* **1998**, *21*, 393−400.

(17) Fair, J. R. Design Aspects for Reactive Distillation. *Chem. Eng.* **1998**, *10*, 158.

(18) Agarwall, R.; Li, Y.-K.; Santollani, O.; Satyro, M. A.; Vieler, A. Uncovering the Realities of Simulation. Part I. *Chem. Eng. Prog.* **2001**, *97*, 42.

(19) Satyro, M. A.; Agarwall, R.; Li, Y.-K.; Santollani, O.; Vieler, A. Uncovering the Realities of Simulation. Part II. *Chem. Eng. Prog.* **2001**, *97*, 64.

(20) Pöpken, T.; Steinigeweg, S.; Gmehling, J. Synthesis and Hydrolysis of Methyl Acetate by Reactive Distillation Using Structured Catalytic Packings: Experiments and Simulation. *Ind. Eng. Chem. Res.* **2001**, *40*, 1566.

(21) DeGarmo, J. L.; Parulekar, V. N.; Pinjala, V. Consider Reactive Distillation. *Chem. Eng. Prog.* **1992**, 43.

(22) Ellenberg, J.; Krishna, R. Countercurrent Operation of Structured Catalytically Packed Distillation Columns: Pressure Drop, Holdup and Mixing. *Chem. Eng. Sci.* **1999**, *54*, 1339.

(23) Sulzer ChemTech Ltd. *Structured Packings for Distillation and Absorption*; Product Information, Sulzer ChemTech Ltd.: Winterthur, Switzerland, 1997.

(24) Kister, H. Z. *Distillation Design*; McGraw-Hill: New York, 1992.

(25) Venkatamaran, S.; Chan, W. K.; Boston, J. F. Reactive Distillation using ASPEN PLUS. *Chem. Eng. Prog.* **1990**, *86*, 45.

(26) Podrebarac, G. G.; Ng, F. T. T.; Rempel, G. L. The Production of Diacetone with Catalytic Distillation. Part II: A Rate-Based Catalytic Distillation Model for the Reaction Zone. *Chem. Eng. Sci.* **1998**, *53*, 1077.

(27) Lee, J. W.; Hauan, S.; Westerberg, A. W. Extreme Conditions in Binary Reactive Distillation. *AIChE J.* **2000**, *46*, 2225.

(28) Górak, A.; Hoffmann, A. Catalytic Distillation in Structured Packings: Methyl Acetate Synthesis. *AIChE J.* **2001**, *47*, 1067.

(29) Kister, H. Z. *Distillation Operation*; McGraw-Hill: New York, 1989.

(30) Castor, J.; Subawalla, H.; Fair, J. R. Preparation of *tert*-Amyl Alcohol in a Reactive Distillation Column. 2. Experimental Demonstration and Simulation of Column Characteristics. *Ind. Eng. Chem. Res.* **1997**, *36*, 3845.

(31) Al-Arfaj, M. A.; Luyben, W. L. Effect of Number of Fractionating Trays on Reactive Distillation Performance. *AIChE J.* **2000**, *46*, 2417.

(32) Nijuis, S. A.; Kerkhof, F. P.; Mark, A. N. S. Multiple Steady States During Reactive Distillation of Methyl *tert*-Butyl Ether. *Ind. Eng. Chem. Res.* **1993**, *32*, 2767.

(33) AspenTech. *Dyna PLUS Reference Manual for Release 2*; Aspen Technology Inc.: Cambridge, MA, 1998.

(34) AspenTech. *SPEEDUP Reference Manual for Release 5*; Aspen Technology Inc.: Cambridge, MA, 1998.

(35) Moritz, P.; Hasse, H. Fluid Dynamics in Reactive Distillation Packing Katapak-S. *Chem. Eng. Sci.* **1999**, *54*, 159.

(36) Alejski, A.; Duprat, F. Dynamic Simulation of the Multicomponent Reactive Distillation. *Chem. Eng. Sci.* **1996**, *18*, 4237.

(37) Kreul, L. U.; Górak, A.; Dittrich, C.; Patron, P. I. Dynamic Catalytic Distillation: Advanced Simulation and Experimental Validation. *Comput. Chem. Eng.* **1998**, *23*, 654.

(38) Luyben, W. L. *Practical Distillation Control*; Van Nostrand Reinhold: New York, 1992.

(39) Bock, H.; Wozny, G.; Gutsche, B. Design and Control of a Reaction Distillation Column Including the Recovery System. *Chem. Eng. Process.* **1997**, *36*, 101.

(40) *Chemical Market Reporter*; Schnell Publishing Company: New York, Jan−Jul, 2002.

Received for review September 12, 2001
Revised manuscript received August 21, 2002
Accepted September 19, 2002

IE010765V